Investigation of flux stability and fouling mechanism during simultaneous treatment of different produced water streams using forward osmosis and membrane distillation.

Investigation of flux stability and fouling mechanism during simultaneous treatment of different produced water streams using forward osmosis and membrane distillation

Muhammad Saqib Nawaz[a], Hyuk Soo Son[a], Yong Jin[a], Youngjin Kim[b], Sofiane Soukane[a], Mohammed Ali Al-Hajji[c], Muhannad Abu-Ghdaib[c], Noreddine Ghaffour[a]

[a] *King Abdullah University of Science and Technology (KAUST), Water Desalination and Reuse Center (WDRC), Division of Biological and Environmental Science and Engineering (BESE), Thuwal 23955-6900, Saudi Arabia, E-mail: noreddine.ghaffour@kaust.edu.sa*

[b] *Department of Environmental Engineering, Sejong Campus, Korea University, 2511, Sejong-ro, Jochiwon-eup, Sejong-si, Republic of Korea*

[c] *Energy Systems Division, Process & Control Systems Department (P&CSD), Saudi Aramco, Dhahran, Saudi Arabia*

Abstract

Forward osmosis-membrane distillation (FO-MD) hybrids were recently found suitable for produced water treatment. Exclusion of synthetic chemical draw solutions, typically used for FO, can reduce FO-MD operational costs and ease its onsite application. This study experimentally validates a novel concept for the simultaneous treatment of different produced water streams available at the same industrial site using an FO-MD hybrid system. The water oil separator outlet (WO) stream was selected as FO draw solution and it generated average fluxes ranging between 8.30 LMH and 26.78 LMH with four different feed streams. FO fluxes were found to be governed by the complex composition of the feed streams. On the other hand, with WO stream as MD feed, an average flux of 14.41 LMH was achieved. Calcium ions were found as a main

reason for MD flux decline in the form of $CaSO_4$ scaling and stimulating the interaction between the membrane and humic acid molecules to form scale layer causing reduction in heat transfer and decline in MD flux (6%). Emulsified oil solution was responsible for partial pore clogging resulting in further 2% flux decline. Ethylenediaminetetraaceticacid (EDTA) was able to mask a portion of calcium ions and resulted in a complete recovery of the original MD flux. Under hybrid FO-MD experiments MD fluxes between 5.62 LMH and 11.12 LMH were achieved. Therefore, the novel concept is validated to produce fairly stable FO and MD fluxes, with few streams, without severe fouling and producing excellent product water quality.

Keywords: Produced water; Oil and grease; FO-MD hybrid; FO and MD fouling; Scaling; EDTA

1. Introduction

In oil exploration activities, a significant quantity of fresh water is injected to facilitate petroleum recovery. After injection, this water returns back to the surface loaded with hydrocarbons, salts and other contaminants commonly known as “produced water” (Xu et al., 2018). This water represents one of the largest streams of process wastewater generated in the industry (Dickhout et al., 2017). Produced water contains a mixture of dissolved and particulate organic and inorganic chemicals, and its characteristics change with time. The quantity produced varies greatly depending on the location and age of the petroleum reservoir. Generally, it is about 7−8 times larger in volume than the oil extracted (Al-Furaiji et al., 2019). However, due to ageing of wells the oil production reduces. Therefore it is estimated that the volume ratio between produced water to oil production may globally ramp up to 12 by 2025 (Jiménez et al., 2018), which will increase the need for efficient produced water treatment strategies.

Crude oil is extracted as a mixture of gas, oil and water and is separated in a three phase separator vessel. The principle of three phase separator is based on gravity, which allows water to settle at the bottom of the separator, then discharged as a wastewater stream; referred as 3PS in this study (Soliman et al., 2020). The salt content of crude oil consists of different salts dissolved in small oil droplets. Refineries desalt crude oil using fresh water or sometimes a mixture of fresh and treated water jointly termed as wash water (WW). The desalting of oil with WW results in the generation of the desalter effluent (DE). This DE is a stable emulsion of oil in water, which must be treated before disposal (Ahmed et al., 2020). After a suitable treatment, produced water can meet stringent environmental standards and reduce the load over fresh water resources (Elmaleh and Ghaffour, 1996; Wenzlick and Siefert, 2020). It can serve as a valuable water resource for various applications including reinjection into the wells. Before reinjection, the produced water is passed through a water oil separator commonly called "WOSEP". A good quality of WOSEP outlet (WO) treated water will eventually improve the receiving ground water quality. A schematic diagram illustrating various produced water streams is shown in **Figure S1** in the supporting information. It can be seen that other waste streams (DE, WW, 3PS, RO reject) contribute to the WO stream volume. Hence its volume can be controlled/reduced by the treatment and reuse of these streams.

The selection of unit operations for the treatment of produced water remains challenging due to its complex composition and the high quality requirements of the treated water (Chang et al., 2019). Microfiltration (MF) or ultrafiltration (UF) of produced water using ceramic or polymeric membranes requires extensive pre-treatment and in some cases also post-treatment to improve the treated effluent quality. Electrodialysis (ED) can remove ionic salts from the produced water, but it cannot remove organics and requires periodic disposal of concentrate (Al-Ghouti et al.,

2019). On the other hand, reverse osmosis (RO) is not a viable solution for the treatment of produced water as RO membranes cannot directly withstand high temperatures associated with produced water which requires extensive cooling before entering the treatment system (Al-Ghouti et al., 2019). Concentration of total dissolved solids (TDS) in produced water may reach 400,000 mg/L which is far beyond the typical salinity limit of RO (~ 70,000 mg/L) (Jiménez et al., 2018). Other distillation techniques like multi-effect distillation (MED) and multistage flash (MSF) can be used for the treatment of highly saline solutions but remain energy intensive and costly processes (Ghaffour et al., 2019). Biological treatment of produced water is only feasible when oil and grease concentration is less than 60 mg/L and chlorides are less than 6600 mg/L (Su et al., 2007). However, chlorides concentration in different types of produced water streams may go up to 250,000 mg/L (Jiménez et al., 2018). Other traditional techniques like hydrocylcone, gravity separation and media filters cannot meet treated water quality that is suitable for recycling and reuse, so sophisticated treatment technologies must be adopted (Bagheri et al., 2018).

Membrane distillation (MD) is considered as a potential technology for produced water treatment. The driving force in MD is the vapor pressure difference between the two sides of the membrane pore, generally triggered by temperature difference between two bulk solutions (Kim et al., 2019a). MD combines the advantages of conventional distillation with membrane filtration. The water that evaporates at the hot feed side (having higher vapor pressure) condenses at the cold permeate side of the membrane (having lower vapor pressure). MD produces water with nearly distilled quality even with nearly saturated saline streams (Al-Furaiji et al., 2019). MD is compact and supposed to be less susceptible to fouling than pressure driven membrane processes (Politano et al., 2017). There are several studies available in the literature

on the use of MD for produced water treatment. The flux in air gap membrane distillation (AGMD) was found directly proportional to the feed temperature and energy consumption was found independent of the membrane pore size (Alkhudhiri et al., 2013). As such, a direct contact MD (DCMD) exhibited 99% inorganics and 90% total carbon removal from produced water (Macedonio et al., 2014). DCMD flux while treating produced water was found inversely proportional to the module length due to the reduction of driving force along the module channel (Xu et al., 2018). The capability of MD to utilize the available low-grade heat, which is generally available in produced water, contributes in reducing the overall energy consumption (Tong and Elimelech, 2016). Among different configurations of MD, the DCMD is most commonly used mainly for its simplicity (Soukane et al., 2021), but other configurations, such as AGMD, possess a higher thermal efficiency (Alsaadi et al., 2015).

Another emerging membrane technology used in desalination of hypersaline solutions is forward osmosis (FO). The FO process utilizes natural osmotic pressure difference across the membrane as the driving force for water transport. The use of a solution of higher salinity (high osmotic pressure), termed as draw solution (DS), enables freshwater recovery from targeted feed solution (FS) of relatively lower salinity, thus lower osmotic pressure (Nawaz et al., 2016). The FO process rejects complex organic and inorganic contaminants present in FS (Kim et al., 2019b). It utilizes energy mainly for recirculation of DS and FS and does not require any hydraulic pressure. However, once DS is diluted with extracted water, its re-concentration (regeneration) is critical to sustain the driving force and ensure the continuous operation of the FO system (Kim et al., 2017).

Hybrid technologies are a combination of more than one technology to enhance benefits in terms of improved water quality, lower operational energy and equipment footprint. Although

RO-MD might be seen as a potential hybrid for the treatment of high concentration streams, it presents potential drawbacks within the scope of produced water treatment. Indeed, RO cannot be fed with WO due to its high temperature and cannot be placed in series with MD due to possible salinity increase in MD output to values as high as 130 g/L. Moreover, RO anti-scalants may have negative impacts on MD flux (Liu et al., 2021; Yan et al., 2017). Recent investigations found FO-MD hybrid system promising for various applications (Arcanjo et al., 2020; Lee et al., 2018; Li et al., 2020; Volpin et al., 2019). In a FO-MD system, the drawbacks of both processes can be reduced by regenerating DS of FO by the MD process and hindering evaporative contaminants, surfactants and trace organics by the FO process (Ghaffour et al., 2019; Xie et al., 2013). The studies available in literature on produced water treatment using FO and MD systems utilize synthetic DS (Al-Furaiji et al., 2019). These DS are prepared by addition of at least one chemical to fresh water to serve simultaneously as DS for FO and FS for MD (Chekli et al., 2017). This requires on-site availability of fresh water and salts, which brings in additional control requirements, equipment and associated operation costs. Therefore, there is a particular need to investigate a more sustainable way that involves no use of fresh water and salts as DS to operate FO-MD for on-site treatment of produced water.

In this study we present a novel concept of simultaneous utilization of different produced water streams, generated at the same site. Depending on the stream characteristics, the produced water could be used as FO FS or DS. The stream with highest TDS and lower oil and grease concentrations could be used as a DS while the relatively diluted streams can be used as FS to recover valuable water, increase their concentration and reduce their volume, thus making them suitable for evaporation or other zero liquid discharge (ZLD) process. The diluted DS will then pass through DCMD for regeneration and produce high quality permeate water. In such a

configuration, FS streams will pass through a double barrier of very selective FO and MD membranes leaving behind most of the contaminants. However, it is also expected that due to the presence of various contaminants in the DS stream, the flux through FO and MD would experience more decline compared to single salt DS (like NaCl only). This study starts with a feasibility assessment of the hybrid concept in treating different produced water streams simultaneously with emphasis on fluxes stability for both FO and DCMD processes. A systematic investigation will follow to identify the dominant mechanism of FO and MD membranes fouling and scaling due to the presence of complex contaminants in the feed and draw streams. The concept is also verified with new integrated FO-MD module which includes a thermal and osmotic dual function isolation barrier (Son et al., 2021). In order to have a better understanding of fouling mechanisms, stable synthetic produced water mimicking the main composition of real produced water collected from a local industrial site is used. This study will serve as a baseline to identify and eliminate any critical factors that can cause flux or permeate quality decline.

2. Materials and Methods

2.1. Formulation of synthetic produced water streams

Five streams were identified from local industrial sites and their samples were collected. The names of streams, abbreviations used in the manuscript, TDS concentrations and osmotic pressures are presented in **Table 1**. Detailed characterization of all five streams, reported in **Table S1** in the supporting information, was performed using advanced analytical techniques and standard methods (APHA, 2006). Based on their TDS concentrations, four streams were selected as potential FS and one “WO” as potential DS for FO.

Table 1: Different produced water streams considered in the study

Stream Name	Stream abbreviation	TDS (mg/L)	Osmotic Pressure* (bar)
Desalter Effluent	DE	6,943	5.6
Water oil separator (WOSEP) Outlet	WO	96,856	74
Wash Water	WW	6,083	4.9
Three Phase Separator	3PS	4,853	3.8
Reverse Osmosis (RO) Reject	RO Reject	6,020	4.8

*Calculated through LENNTECH online osmotic pressure calculator (https://www.lenntech.com/calculators/osmotic/osmotic-pressure.htm)

Based on the detailed characterization results, the composition of synthetic produced water was established (see first part of **Table 2**). All elements present in real streams were added in similar molar concentrations. Glucose was added to represent chemical oxygen demand (COD) concentration and colloidal silica to represent mainly the turbidity and total suspended solids (TSS) concentration. The standalone FO experiments were carried out using the composition in **Table 2** without adding oil and grease to estimate the effect of other parameters on the flux. However, in integrated FO-MD experiments, exact oil and grease concentrations were used for all 5 streams. Part two of **Table 2** lists the three chemicals which were used only for the systematic investigation of MD membrane fouling in standalone MD experiments. Maximum oil and grease concentration in any stream was found to be 32 mg/L (**Table S1**) that is why a range of 30-50 mg/L was studied to mimic a worst case scenario. The oil used was a standard emulsion of oil in water with tiny droplets to mimic the most challenging type of oil presence. Humic acid

(HA) is used as model foulant for natural organic matter. A HA concentration range of 20-80 mg/L was selected following similar investigations (Khan et al., 2019; Lee et al., 2020). Similarly, EDTA is considered as a masking agent for the bivalent metals. Hence it was also used in the concentration range 0.001 M to 0.0005 M as described elsewhere (Kim et al., 2020). However, in the integrated FO-MD experiments HA and EDTA were not added. The synthetic streams were always freshly prepared prior to each experiment. All chemicals were of reagent grade and were received from Sigma Aldrich, Fisher Scientific or Alfa Aesar and used without any additional processing.

Table 2: The composition of different synthetic produced water streams

Chemical	**DE**	**WO**	**WW**	**3 PS**	**RO reject**
Concentration used in standalone FO and FO-MD integrated experiments (mg/L)					
NaCl	1,863	62,974	1,118	1,045	213
KCl	232	2,955	207	130	164
$CaCl_2$	1,873	23,358	1,667	1,466	1,964
$MgCl_2$	505	4,074	501	626	940
Na_2SO_4	2,305	2,054	2,438	1,478	2,704
$BaCl_2$	0.19	3.24	0.12	3.91	0.18
$SrCl_2$	33	729	20.4	28.96	25.3
Glucose	77	642	77	44	5
Silica colloids (0.3 µm)	50	60	50	0	0
Oil and grease (for FO-MD integrated experiments only)	5	7	0	32	5
Additional compounds for fouling studies on standalone MD					
Chemical	**Chemical properties**			**Concentration (mg/L)**	
Humic acid sodium salt	Powder (50-60% as humic acid)			20, 60, 80	
Oil and grease	Standard solution (1000 mg/L)			30, 40, 50	
EDTA	(99% pure) MW =292.23 g/mol			292, 146	

2.2. FO and MD membranes

For the FO experiments, thin film composite polyamide (TFC-PA) hydrophilic FO membranes were used. The membranes were purchased from Toray Chemicals, Korea. The thicknesses of the active and support layers are 0.86±0.1 and 99.14±1.3 μm, respectively. The support layer porosity is 63±5%. Water permeability of the FO membrane (A_{FO}) is 2.472E^{-7} m/s/bar, solute permeability (B_{FO}) is 5.444E^{-8} m/s, and structure parameter (S_{FO}) is 3.28E^{-4} m. Additional details on this membrane can be found elsewhere (Lee and Ghaffour, 2019).

In MD experiments, polytetrafluoroethylene (PTFE) hydrophobic microporous membranes purchased from Membrane Solutions, China were used. The measured nominal pore size and porosity are 0.22±0.06 μm and 39.59±4.7 %, respectively. Thicknesses of the active layer (PTFE) and the support layer (PP) are 20±0.4 and 80±1.6 μm, respectively, and the liquid entry pressure (LEP) is 3.74 bar. The membranes size was 6 cm × 1.6 cm for both FO and MD modules which gives an active area of 0.00096 m^2.

2.3. Experimental setups and procedures for standalone FO and MD experiments

Two laboratory-scale setups were installed for FO and MD. Equipment source and models were generally the same for both setups. Schematic diagrams of standalone FO and MD batch setups are shown in **Figure S2a** and **S2b**, respectively. The FO setup consists of two variable-speed gear pumps (75211-70, Cole-Parmer, USA), a standard membrane cell, a weighing balance (ME3002E, Mettler Toledo, USA) and a temperature controller with water bath and heat exchangers (AD07R-20-A13D, PolyScience, USA). The membrane cell has two symmetric channels (i.e., 60 mm long, 16 mm wide and 3 mm deep) on both sides of the membrane. One channel was fed with the feed stream and the other was fed with a draw stream. Variable speed gear pumps were used to provide crossflows under counter-current directions. The flowrate was

set to 250 mL/min which gives a fluid average crossflow velocity of 8.7 cm/s. Initial FS temperature was at laboratory temperature (22±2 °C) while the DS temperature was maintained at 40 °C throughout the experiment. The latter was found to be the optimum temperature for DS and it is achievable in large scale MD feed outlet temperature (Lee and Ghaffour, 2019; Volpin et al., 2019). Both solutions were recirculated in a closed-loop system resulting in a batch mode process operation. The DS tank was placed on a digital weighing balance and the weight changes were recorded. The FO experiments were carried out for 20 h, with an initial volume of 1 L for both DS and FS. A new membrane coupon was used for each experiment, after which it was air dried and stored for imaging and characterization purposes. The conductivities of both feed and DS were recorded. In all FO experiments, an active layer facing the DS (AL-DS) mode was used because the draw stream had very high TDS compared to the feed streams.

The lab-scale DCMD set-up (**Figure S2b**) is composed of two variable-speed micro gear pumps, a standard membrane cell, a digital weighing balance and two temperature controllers. The membrane cell has two symmetric channels (i.e., 60 mm long, 16 mm wide and 3 mm deep) on both sides of the membrane. One was fed with MD feed and the other was fed with MD permeate (DI water). Initial volumes of both MD permeate and feed were set to 1 L each. In all MD experiments the active layer was facing MD FS. Different FS temperatures were used while the permeate temperature was maintained at 20 $^{\circ}$C. Both feed and permeate temperatures were measured at the inlet of the module using sensors. MD experiments were continued until negligible flux (below 2 LMH) was observed. A new membrane coupon from the same original sheet was used for each experiment, after which it was air dried, cut into two parts (one was rinsed with DI water for two minutes and the other left without rinsing) and stored for imaging and characterization. The conductivity of permeate solution was measured with a conductivity

meter (TetraCon 325 with LF 298, WTW, USA) to monitor any salt leakage through MD membrane. Additionally, the pH of both feed and permeate solutions were measured at the beginning and after completion of the experiment. The COD of permeate was also measured using Hg free HACH vials (3-150 mg/L range) to assess any leakage of volatile organics through the membrane. For membrane surface characterization, the stored dried membranes were analyzed by scanning electron microscopy (SEM) (Gemini II, Carl Zeiss SMT AG, Germany) and energy dispersive X-ray spectroscopy (EDX) at an accelerating voltage of 3 kV and 20 kV, respectively.

2.4. Experimental setups and procedures for integrated FO-MD experiments

An in-house designed integrated FO-MD module with an osmotic and thermal isolation barrier, as depicted in **Figure 1**, is used in this study (Kim et al., 2019a). The integrated module has four symmetric channels, 100 mm long, 20 mm wide and 3 mm deep. The top channel was fed with FO FS and the bottom channel with MD permeate. The middle channels were fed with MD FS which also serves as FO DS. Similar to the batch experiments, MD FS temperature was maintained at 60 $^{\circ}$C while MD permeate was set at 20 $^{\circ}$C. Regarding FO, the FS was initially at laboratory temperature (22±2 $^{\circ}$C). Similar to standalone experiments, the AL-DS configuration was used for FO membrane and AL-FS (MD FS) configuration for the MD membrane. Countercurrent cross flow velocities were maintained at an average of 8.7 cm/s with a 315 mL/min flow rate. The operating principle of the integrated FO-MD module with the barrier, consists of flowing first the DS at 60 $^{\circ}$C into the channel as MD FS (at one side of the barrier) to fully utilize its heat and maximize the MD flux. The same relatively concentrated DS (after losing some heat and vapors to MD permeate) flows to the other side of the isolation barrier,

where it serves as FO DS (**Figure S3**). Starting volume of both FO FS and FO DS was 1 L while MD permeate was 0.5 L. Experiments were continued until either FO or MD flux reached a constant minimum value (below 2 LMH). Composition of WO and other streams was kept exactly as reported in part 1 of **Table 2**.

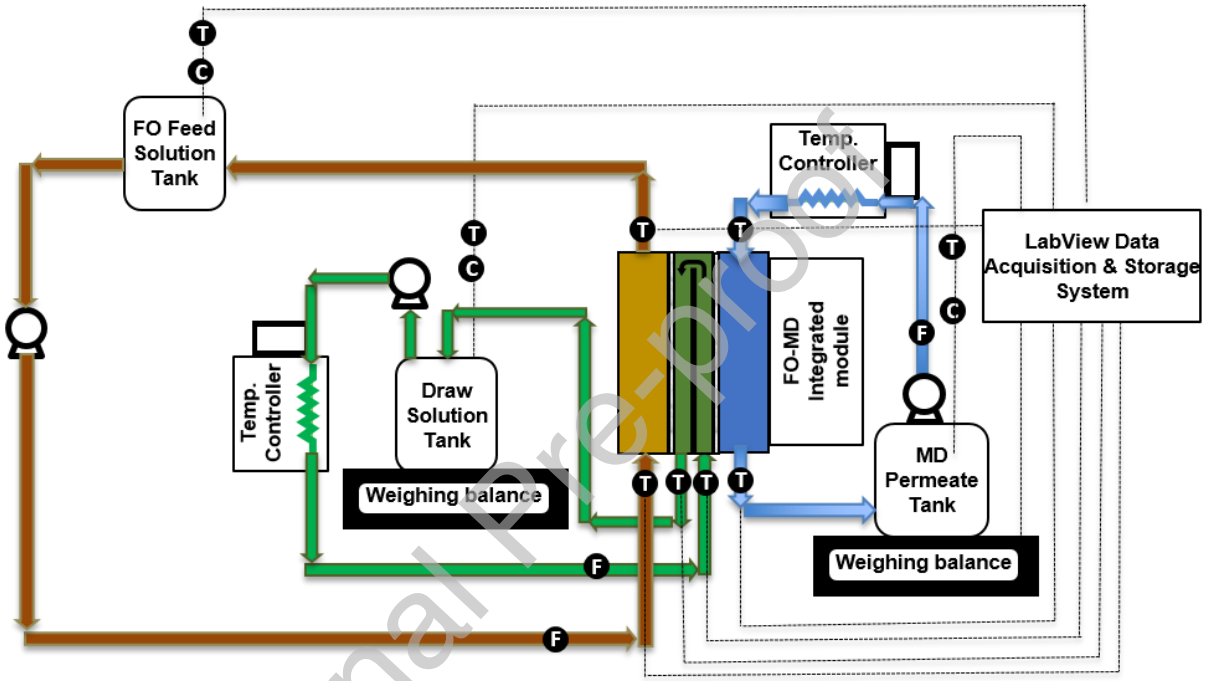

Figure 1: Schematic diagram of integrated FO-MD setup used in this study.

2.5. Calculation of salt transfer across the FO membrane

The salt transfer across the membrane was estimated by continuously monitoring the actual conductivity values of the FS and DS. Calculated values of conductivities were estimated with the assumption of zero salt transfer across the membrane and represent the actual initial conductivity divided by the cumulative volume of FS or DS at the end of the experiment. These calculated values were subtracted from the actual conductivities to estimate the amount of salt

transferred. However, regarding the FS, any increase in the conductivity was either due to RSF or increase in the bulk FS temperature. The increase due to temperature was calculated using Eq. (1), and the remainder was attributed to RSF. The specific RSF (SRSF) was obtained by dividing the RSF by the flux. It is important to mention here that, due to the assumptions made above the SRSF values cannot be 100% correct and some margins of error must be kept into account.

(1) $EC = [\ 1 + a\ (t - 25)\ ]\ EC_{25}$ with $a = 0.020$

3. Results and Discussion

3.1. Flux stability and membrane fouling/scaling in standalone FO

In order to carry out a complete experimental validation of the concept, all four streams (DE, WW, 3PS, RO Reject) were separately used as FO FS with "WO" as DS. Since all the experiments were executed under the same initial operating conditions (as described in section 2.3), the difference in flux could be attributed to the composition of the different feed streams.

As shown in **Figure 2**, a sharp decline of water flux was observed between the 1st h and 6th h of operation for DE, 3PS and WW, followed by gradual flux stabilization, achieved after 10th h. This initial sharp decline was mainly due to the dilution of DS and loss of osmotic potential. However, for RO reject feed, the flux showed a continuous decline, almost linearly during the whole experiment with an overall highest flux compared to the other streams. This could be attributed to the absence of silica colloids and low concentration of sodium chloride in the RO reject (see **Table 2**). Silica colloids are found to make polymerized silica layer after interacting with TFC PA membrane on which it attaches firmly due to the Si-O bond (Kim et al., 2020). However, comparing the compositions of 3PS and RO reject, silica is absent in both solutions and the TDS concentration of 3PS is lower than RO reject (4.85 vs 6.02 g/L) but still the average

flux of RO reject is higher (26.78 LMH) compared to 3PS (14.75 LMH). The main difference in their compositions is the high NaCl concentration in 3PS (1045 mg/L) compared to RO reject (213 mg/L). In AL-DS configuration a polarized layer is established inside the porous support layer of FO membrane due to the diffusion of smallest radius monovalent salts like NaCl, leading to internal concentration polarization (ICP) which reduces the overall flux (Lee et al., 2020). Thus ICP caused by monovalent salts is probably the first main reason for the FO flux decline. Furthermore, RO reject is expected to have less fouling compared to other streams because of its advanced pre-treatment prior to the RO process, which may explain the absence of the sharp decline of the initial FO flux.

Looking at the SEM image in **Figures 3b** and EDX image in **Figure S4b** (supporting information), while using DE as FS, the calcium silicate layer can be observed on the support layer, completely covering the membrane surface. Similar appearance of calcium silicate can be observed on the support layer along with sodium chloride crystals when using WW as FS, see **Figure 3d** and **Figure S4d** (supporting information). It has been reported earlier that silica colloids can cause serious homogeneous and heterogeneous nucleation over the membrane surface and cause a flux decline by pore blocking (Bell et al., 2017; Kim et al., 2020). In the present study, this layer is found as deposits on the polysulfone support layer side which resulted in a net decline in osmotic pressure gradient causing an overall flux decline. 3PS has higher flux than WW and DE because it has no silica to form colloid scale layer, as discussed above. Therefore, colloidal scaling on the support layer surface is the second reason for the FO flux decline.

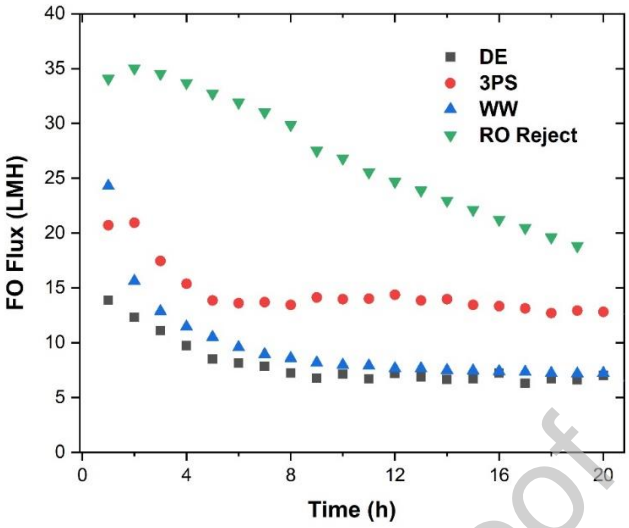

Figure 2: Fluxes using different FO feed streams with the same WO stream as DS. Operating conditions: Initial volume of DS=FS = 1 L, DS temperature = 40 °C, FS temperature 22±2 °C, Crossflow velocity = 8.7 cm/s (250 mL/min), Counter current, AL-DS configuration.

The TFC FO membranes used in this study have an active polyamide layer which is more hydrophilic and negatively charged to produce higher nutrient and micro pollutant removal (Viet et al., 2019). This negative surface charge and electrostatic repulsion may result in the attachment of positive ions to the membrane surface (Chekli et al., 2018). The WO DS used in this study contains several positively charged ions, thus NaCl and $CaSO_4$ crystals can be seen on active layers of all experiments presented in the SEM images (**Figure 3 (a,c,e,g))** and EDX images (**Figures S4 (a,c.e,g))** in the supporting information. The calcium ions can have interfacial interactions with carboxylic groups of polyamide and it can serve as a bridge between various foulants and membrane active layers (Gou et al., 2018). The attachment of calcium ions on the active layer can stimulate $CaSO_4$ scaling (Kim et al., 2020; Xie and Gray, 2016). It is

interesting to note that with RO reject as FS, $CaSO_4$ was present on both sides of the membrane surface as shown in SEM images in **Figures 3g** and **3h** and EDX images in **Figures S4g** and **S4h** (supporting information). Though, crystals are more pronounced on the active layer. One main reason for this could be an inverse relationship between solubility of calcium sulfate (as gypsum) and temperature in an aqueous solution containing higher concentrations of chlorides (Li and Demopoulos, 2006; Zarga et al., 2013). As draw streams have a relatively higher temperature of 40 $^{\circ}$C compared to the feed streams (22±2 $^{\circ}$C), more insoluble $CaSO_4$ was available for crystallization over the active layer. Another reason could be the presence of almost 10 time higher concentration of calcium ions in WO compared to the FS. Among other foulants, NaCl crystals were mostly observed on the active layers as seen in SEM images in **Figure 3 (a,c,e,g)**. Thus, the third main reason for the FO flux decline is most probably the $CaSO_4$ and NaCl crystals deposition on the active polyamide layer causing diluted ECP. The fouling characteristic of an FO process with produced water shows that niche pre-treatment technologies for calcium and silicon removal can be introduced for sustainable operation.

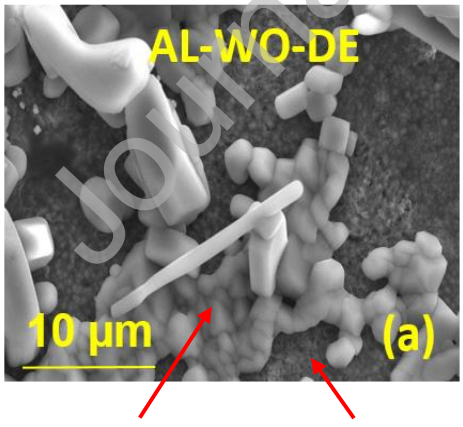

NaCl crystals homogenous nucleation and $CaSO_4$ traces

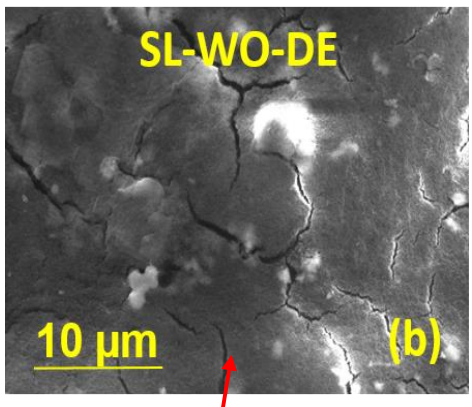

$CaSiO_3$ scale layer

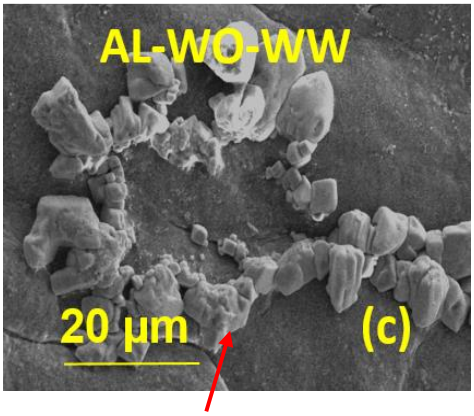

NaCl crystals

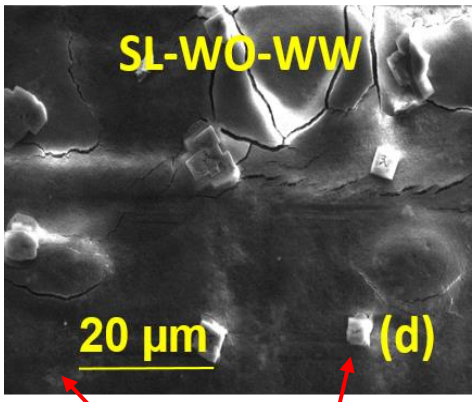

$CaSiO_3$ layer and NaCl crystals

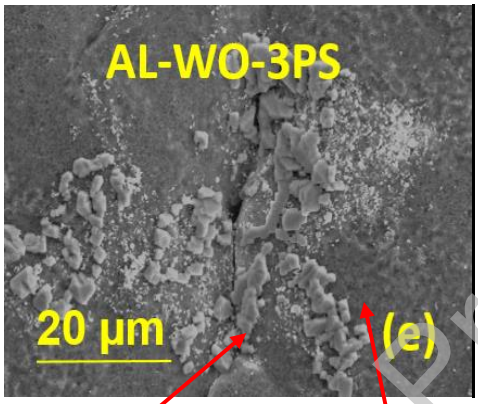

NaCl crystals homogenous nucleation and $CaSO_4$ traces

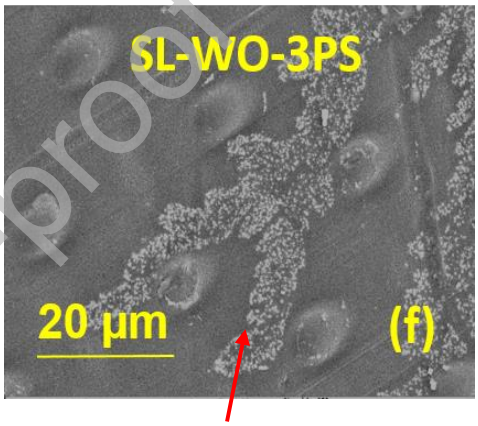

NaCl

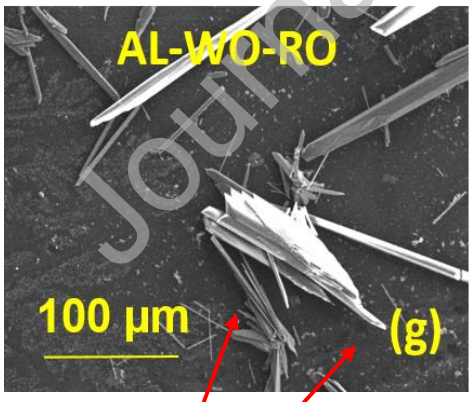

$CaSO_4$ crystals and NaCl traces

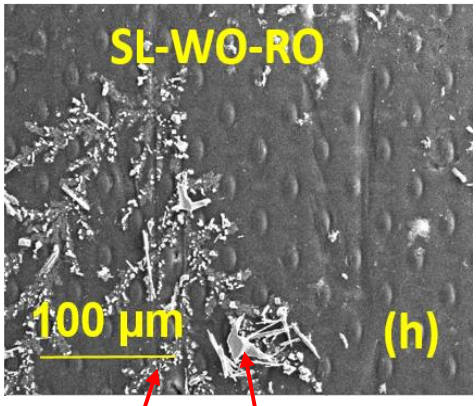

NaCl and $CaSO_4$ crystals

Figure 3: SEM images of active layers (AL) and support layers (SL) of FO experiments with different feed streams (a) AL-WO-DE, (b) SL-WO-DE, (c) AL-WO-WW, (d) SL-WO-WW, (e) AL-WO-3PS, (f) SL-WO-3PS, (g) AL-WO-RO, (h) SL-WO-RO.

3.1.1. Salts transfer across the FO membrane

It was noted that the actual FS conductivity was always greater than the calculated conductivity for all cases. **Table 3** shows the values of cumulative gain of conductivities for the FS and DS in all four FO experiments. This increase may be attributed to the increase of FS temperature from its initial inlet value of 22 ± 2 °C to 27 ± 1 °C as depicted in **Figure 4.** Since the operating temperature of FO DS was maintained constant at 40 °C, it caused heat transfer across the membrane and heated up the feed streams in the first two hours to reach thermal equilibrium around 27 ± 1 °C. This heat transfer triggered intermittent heating and caused a positive fluctuation in the DS temperature and an increase in its actual conductivity. The FS and DS conductivities increased due to increase in the dissociation constant of different salts and reduction in the viscosity of water. Using linear interpolation (**Eq. 1**) the average increase in conductivity is about 2% per degree Celsius increase in temperature.

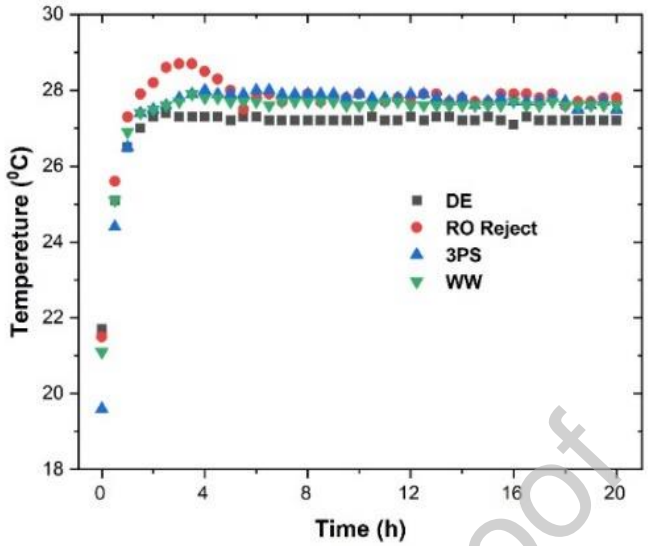

Figure 4: The FS temperature profiles in FO experiments with different feed streams.

Looking at SRSF values in **Table 3** one can notice that the RO reject had the smallest value (0.60) because it was the stream with lowest concentration of monovalent salts that contribute easily towards ICP. So, SRSF was found directly proportional to the concentration of monovalent salts in the FS. Bell and co-workers (Bell et al., 2017) reported similar results and concluded that with higher scale layer formation on the feed side, the negatively charged ions of the layer attracts the positive ions from the DS, which increases the RSF. Similarly, anion RSF from DS is found to interact with the cations in the FS to cause severity of fouling and flux decline (Li et al., 2015). The negative impact of RSF can be found in the form of increased fouling propensity, loss of DS and osmotic pressure (Akther et al., 2015). Therefore, the fourth main reason for FO flux decline can be attributed to RSF triggered by the higher concentration of monovalent salts in the FS.

Table 3: Average fluxes and conductivity transfer estimation in FO experiments with different FS

Description	DE	RO Reject	3PS	WW
Avaerage flux (LMH)	8.30	26.78	14.75	10.29
Cumulative volume extracted in 20 hrs (mL)	153	504	279	187
Cumulative gain in conductivity of FS in 20 hrs (µS/cm)	3,829	3,581	4,840	4,639
Potential increase in FS conductivity due to temperature gain (µS/cm)	1,310	2,023	1,465	1,387
Remaining increase in FS conductivity due to RSF (µS/cm)	2,519	1,558	3,374	3,251
SRSF (g/L)	1.70	0.60	1.60	2.10
Cumulative gain in conductivity of DS in 20 hrs (µS/cm)	3,702	5,669	8,690	4,257

From the discussion of section 3.1, it can be concluded that the concept of simultaneous treatment of different produced water streams can generate fairly stable FO fluxes which are comparable to the fluxes reported in the literature for similar types of feed streams (Al Hawli et al., 2019; Bhinder et al., 2015). The fluxes were found mainly dependent on the composition of feed streams. Furthermore, it can be inferred that ICP caused by the monovalent salts in the FS was the first main reason for flux decline. Colloidal calcium silicate scaling on the support layer side was the second main reason. The dilutive ECP on the active layer side caused by the $CaSO_4$ and NaCl crystals deposition was the third main reason for flux decline. Finally, the RSF from the DS triggered by the concentration of monovalent salts in the FS was the fourth main reason for flux decline during simultaneous treatment of produced water streams.

3.2. Flux stability and membrane fouling/scaling in standalone MD

3.2.1. Effect of MD feed temperature

In order to further validate the concept of simultaneous treatment of produced waters, the use of WO as MD FS must be able to yield a practical and stable flux. MD experiments were operated with WO stream and NaCl solution (with a TDS concentration similar to that of WO around 97 g/L) as FS (**Figure 5a**). NaCl FS was used as a reference to assess the severity of scaling and fouling while treating WO as MD FS. The initial fluxes of both WO and NaCl, respectively, were the same at different temperatures (15.61 and 15.63 LMH at 60 $^{\circ}$C, and 23.2 and 22.78 LMH at 70 $^{\circ}$C) before declining at different concentration factors. The gradual decline in fluxes with NaCl is most probably attributed to the decline of vapor pressure with time due to the increase of feed concentration. The average fluxes for NaCl after 20 h operation were 22.34 and 16.10 LMH with final fluxes of 20.8 and 15.67 LMH at 70 $^{\circ}$C and 60 $^{\circ}$C, respectively. No membrane wetting was observed (**Figure 5b**) and a concentration factor of about 2.3 (65% water recovery) was achieved. Since there was no other contaminant present in the FS and flux was quite stable, it can be inferred that NaCl is not the flux limiting factor in the MD system under our experimental conditions. Our findings are in accordance with the findings of Viet and co-workers (Viet et al., 2020) who revealed that monovalent ions like sodium can interact with organic functional groups and form aggregates but they do not normally deposit over the membrane surface and hence flux is not much affected. Clean membrane with very little NaCl traces can be seen in the SEM image in **Figure 6a** and EDX image in **Figure S5a** (supporting information).

The average MD fluxes for WO (20 h operation) were 8.90, 14.41 and 12.06 LMH with initial fluxes of 11.19, 16.56, 23.20 LMH and final fluxes of 7.97, 12.26, 0.20 LMH for 50, 60 and

70 °C, respectively. As shown in **Figure 5a**, WO also showed the best performance in terms of flux at 60 °C where the concentration factor up to 1.56 (28% recovery) was achieved. A sudden drop in flux observed at 70 °C may be attributed to the formation of a scaling layer over the membrane surface leading to lower final flux than 60 °C. SEM image presented in **Figure 6b** and EDX in **Figure S5b** (supporting information) shows the deposition of calcium sulfate crystals on the membrane surface. This reduction in flux could occur mainly due to the partial blockage of the membrane pores or by the formation of a scaling layer on the membrane surface (Lee et al., 2020). In our study it shows more of a partial blockage of membrane pores. $CaSO_4$ solubility is expected to be inversely proportional to the solution temperature under experimental conditions of high chlorides concentration in the WO solution (Li and Demopoulos, 2006). That is why at higher temperature (70 °C), more scaling was observed due to reduced solubility and more crystallization which caused a flux decline. Similar results were observed by (Lee et al., 2018) while investigating Red Sea water MD scaling using in-situ OCT technique (VCF ranging between 1.2-3.2 and 1-4.5, respectively).

As WO also contains about 63% NaCl (by weight) and we noted in reference experiments that NaCl is not the flux limiting factor under our experimental conditions, therefore, the main reason for inorganic scaling in MD could be attributed to the $CaCl_2$ that was present by about 23% (by weight) in the WO solution. The divalent calcium ions from $CaCl_2$ have higher hydration radius and more positive charge to cause concentration polarization over the membrane surface. No membrane wetting was observed and conductivity and COD results show >99% rejection (**Figure 5b** and **Table 4**) of different inorganic and organic contaminants. Moreover, from the SEM images of **Figure 6c,** it can be observed that the crystal attachment is loose and can easily be removed by simple rinsing with the DI water as also observed recently in another study (Kim

et al., 2020). Due to relatively better flux caused by less scaling propensity, 60 °C was selected as the optimum operating temperature for the remaining experiments. Similar temperature has also been regarded as an optimum for MD operations (Gryta, 2020; Hou et al., 2015). The average flux achieved in our study (14.41 LMH) at 60 °C is comparable to the fluxes reported elsewhere under similar operational conditions (Gryta, 2020; Ricceri et al., 2019).

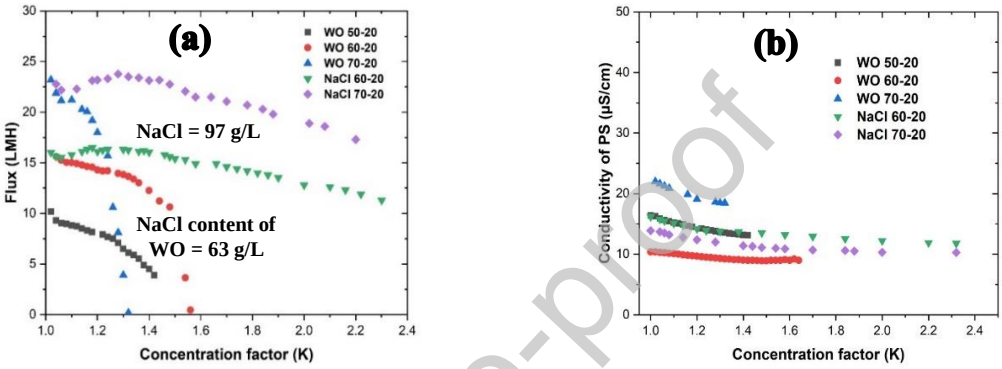

Figure 5: Effect of FS temperature and composition on (a) MD flux, (b) Conductivity of permeate.

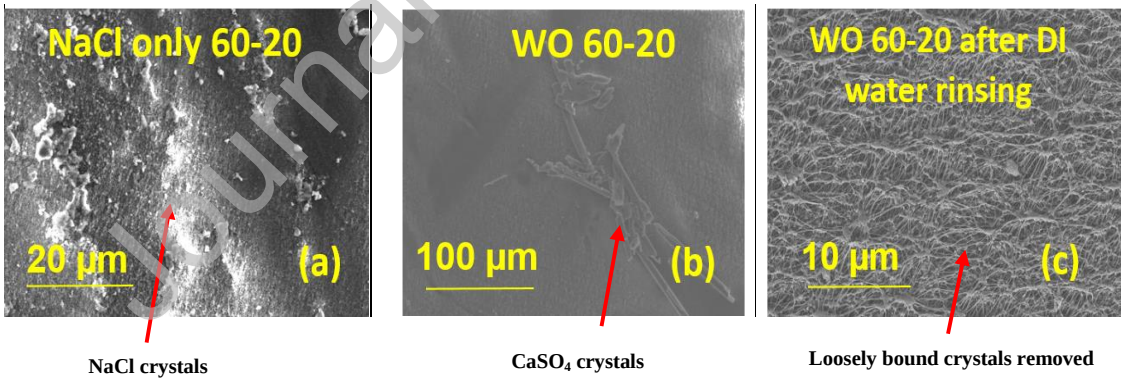

Figure 6: SEM images of MD membranes active layers under different conditions (a) NaCl only at 60-20 °C, (b) WO at 60-20 °C, (c) WO 60-20 °C after DI water rinsing.

3.2.2. Effect of humic acid

To understand the MD membrane fouling mechanism, the effect of HA addition on the MD flux and permeate quality was investigated. HA is found in aquatic environments as natural organic matter (NOM) and is considered as a main organic foulant in MD (Khan et al., 2019; Lee et al., 2020). Different concentrations of humic acid (20, 60 and 80 mg/L) were added to WO FS. The concentration range was selected following an earlier investigation by Hou and co-workers (Hou et al., 2015). The effect of HA on MD flux and permeate conductivity is reported in **Figures 7a** and **7b**, respectively. It was observed that the DCMD flux reduces by 6% with 20 mg/L HA compared to the flux generated by the WO solution alone. The initial and final fluxes were 16.59 LMH and 0.19 LMH, respectively, with maximum concentration factor of 1.44. It is expected that due to the low operating pressure of MD, the HA aggregates on the membrane surface in less compact layers which can be single or double. However, from the **Figure 8c** a homogenous single layer can be observed. HA fouling may become severe in the presence of divalent calcium ions as it can act as a binder between carboxylic groups of two HA molecules (Hou et al., 2015; Khan et al., 2019). Therefore, one can reassert the known fact that the HA layer thickness is not governed by the concentration of HA in the feed stream but by the concentration of calcium ions in the solution instead. That is why almost similar flux trends were observed with different concentrations of HA (20, 60 and 80 mg/L), while the concentration of calcium ions was the same.

Moreover, calcium ions also have the ability to reduce the electrostatic repulsion between HA molecules and PTFE membrane to facilitate its attachment on the membrane surface. As calcium ions were significantly present in the WO solution, their role in enhancing the effect of HA fouling cannot be ignored. HA also have the ability to migrate through membrane pore via adsorption-desorption mechanism by hydrogen bonding between water and HA (Laqbaqbi et al.,

2017). However, in this study the conductivity and COD of permeate solution (**Table 4**) remained unchanged which confirms a complete membrane selectivity to HA and the impact on flux was limited to the surface fouling only. As shown in SEM image in **Figure 8a** and EDX image in **S5c** in supporting information, the $CaSO_4$ crystals can also be seen on the membrane surface.

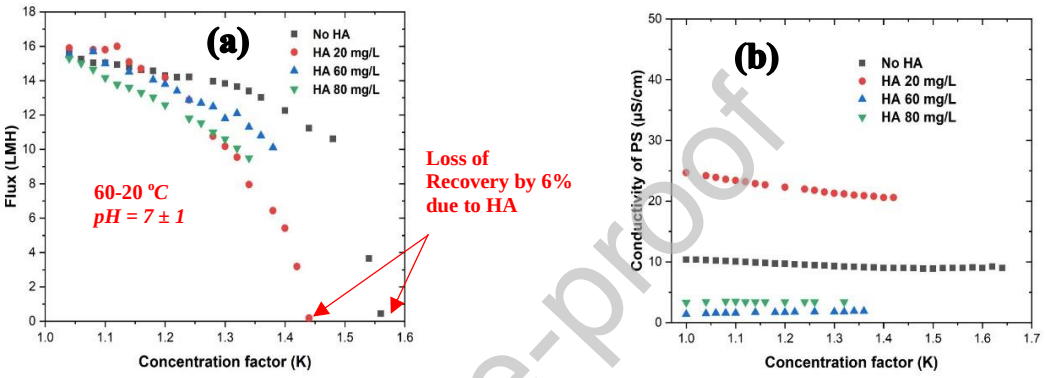

Figure 7: Effect of humic acid on (a) MD flux (b) conductivity of permeate.

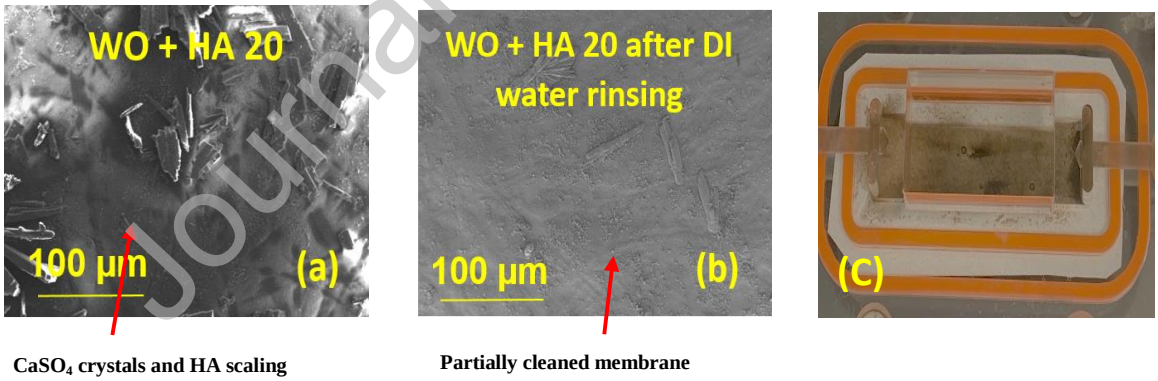

Figure 8: (a) SEM image of active layers with WO + HA20, (b) SEM image of active layer after rinsing with DI water, (c) single homogenous HA layer deposit over the membrane after experiment completion.

The addition of HA probably resulted in more tenacious crystals compared to loosely bound crystals observed without HA. That is why rinsing with DI water was not that much effective, as extensively investigated (Kim et al., 2020), and traces can be found over the membrane surface in the SEM image of **Figure 8b**. Thus, co-presence of calcium ions and humic acid in the solution is likely the main reason for tenacious $CaSO_4$ crystals.

3.2.3. Effect of oil and grease

In the next stage of the investigation on the fouling mechanism and flux, the effect of oil and grease was evaluated. Hydrophobic membranes are prone to fouling by the oil due to strong hydrophobic-hydrophobic interactions. The low surface energy of these membranes accelerates the pore wetting process. Oil and grease are unique foulants and cannot be treated like solid particle, of which shape does not change under MD operating pressure. In fact oil droplets can deform and cleave to pass through membrane pores which are technically smaller than their sizes. In MD, oil droplets are less prone to deformation than in pressured membrane processes (Ghaffour and Qamar, 2020). Oil in wastewater can appear in three different states based on droplet size, namely free oil (>150 µm), dispersed oil (20-150 µm) and emulsified oil (<20 µm) (Tanudjaja et al., 2019). Actually, all larger size droplets can easily be removed through floatation and separation processes while the smaller emulsified oil droplets remain difficult to eliminate and may affect the MD process. Fouling with oil droplets can occur either in the form of a hydrophobic layer above the actual membrane active layer or through partial or complete pore blocking. While the oil layer can seriously affect the flux through the MD system, the membrane wetting can allow non-volatile salts to cross the membrane and contaminate the permeate solution to ultimately deteriorate its quality.

From **Figure 9a** it is observed that addition of oil causes further reduction in the overall flux to curtail the concentration factor to 1.40 (20% recovery) with initial and final fluxes of 18 LMH and 1.4 LMH, respectively. This is approximately 2% less flux compared to the case where WO with HA (20 mg/L) was used as MD feed. Although no wetting was observed, oil traces can be seen to partially cover the membrane surface even after rinsing with DI water, as shown in **Figure 10b.** Also in the SEM image of **Figure 10a** and the EDX image of **Figure S5d** (supporting information) the oil can be seen as carbon deposits over the surface of $CaSO_4$ crystals. Same results of partial pore clogging by oil while using almost similar oil concentration (40 mg/L) were observed by other researchers (Gryta, 2020; Han et al., 2017). Therefore, predominantly the oil and grease fouling mechanism in our experimental conditions was attributed to partial pore clogging, which did not affect the flux severely. The MD experiments presented in this study indicate that the range of oil and grease concentration in the produced water samples allows further application of MD processes. On the other hand, the impact of partial fouling shown in the results requires further investigation for long term operations.

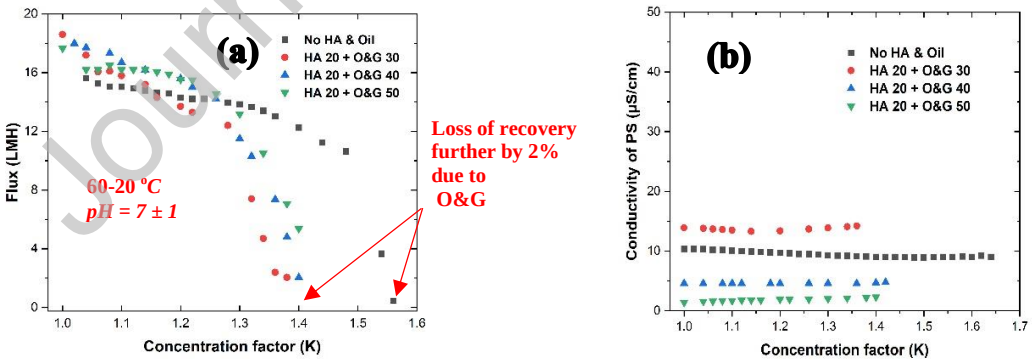

Figure 9: Effect of oil and grease on (a) MD flux (d) conductivity of permeate.

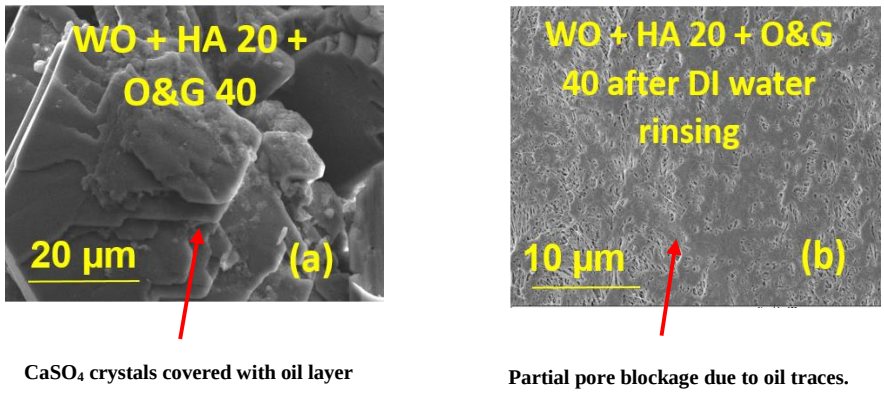

Figure 10: SEM images of active layers of MD membranes (a) with oil and grease and (b) after rinsing with DI water.

3.3. MD flux recovery with EDTA

EDTA is a well-known hexa-dentate ligand that has the intrinsic ability to attach metals and form chelates. Additionally, EDTA and its derivatives are supposed to be part of a fouling mitigation strategy against divalent cations especially calcium. Ding and co-workers (Ding et al., 2020) used ethylenediamine tetra (methylenephosphonic acid) sodium salt (EDTMPA-Na) as a FO DS and observed that its RSF into the FS reduces effectively the formation of calcium sulfate scales on the membrane surface. Therefore, two different concentrations of EDTA (0.001 M and 0.0005 M) were added to the WO solution already containing 20 mg/L HA and 40 mg/L oil and grease. Interestingly, a complete flux recovery was observed with 0.001 M EDTA as shown in **Figure 11a.** The concentration factor of 1.58 was achieved with initial and final fluxes of 16.94 and 0.32 LMH, respectively. One reason for this could be the masking of some of the calcium ions in the EDTA complex which reduced their negative impact on flux. That is why more flux recovery was observed with higher concentration of EDTA (0.001 M) and almost no recovery was observed with lower concentration (0.0005 M) leading to a maximum concentration factor of 1.38 Further higher concentrations of EDTA (>0.001 M) were not tested because it is not

economically feasible. Moreover, since 0.001 M EDTA can bring the pH of WO solution to 3.5, a higher concentration will make it even more acidic. The drop in pH can reduce the dissociation of HA and reduce its chances for adsorption on the membrane (Hou et al., 2015); hence this might be the second reason for flux improvement with EDTA addition. In same study on DCMD, EDTA was found effective to reduce HA fouling by the removal of calcium ions (Hou et al., 2015). The mechanism of Calcium ion entrapment by EDTA is presented by Li and co-workers (Li et al., 2019) and is reproduced in **Figure 12c**. The $CaSO_4$ crystals along with NaCl crystals can be observed in SEM images in **Figure 12a** and EDX image in **Figure S5e** (supporting information). Rinsing with DI water was not effective to completely remove the tenacious crystals from the membrane surface. Hence, it can be concluded that EDTA can recover the flux by partially masking the divalent ions specially the calcium ions and by reducing the dissociation of HA. However, it cannot halt oil and grease from causing partial membrane clogging.

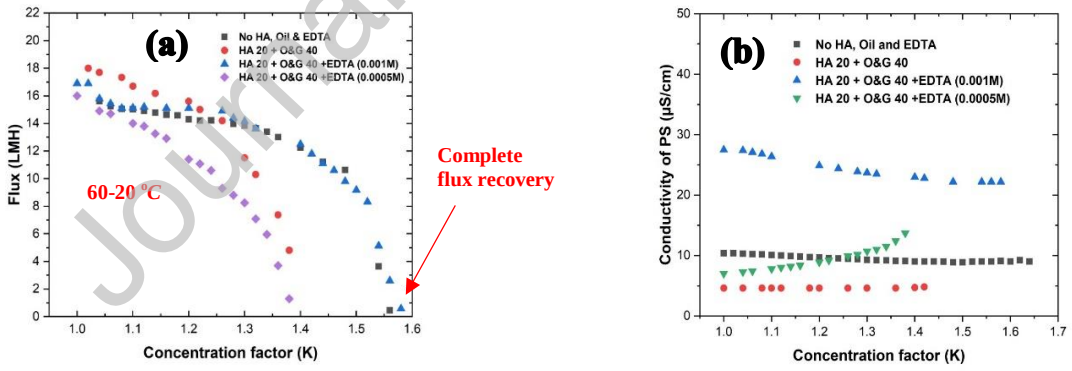

Figure 11: Effect of EDTA on (a) MD flux recovery and (b) conductivity of permeate.

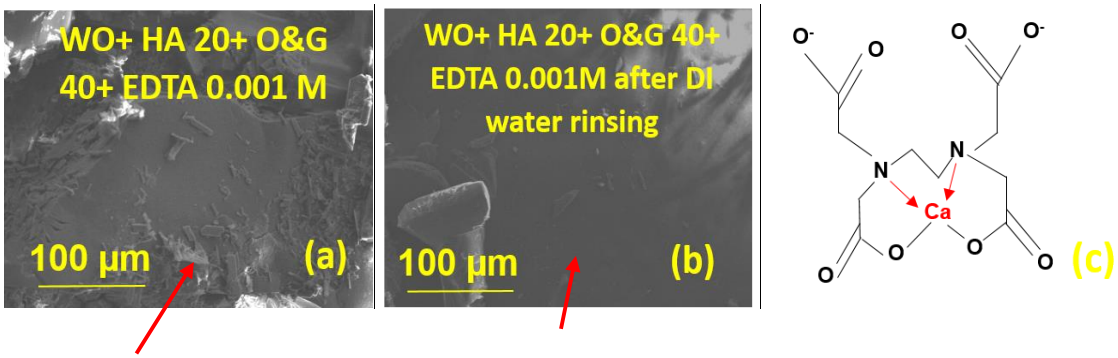

This figure will be changed

$CaSO_4$ crystals

Figure 12: SEM images of active layers of MD membranes (a) with EDTA and (b) after rinsing with DI water.

3.4. FO and MD fluxes through Integrated FO-MD system

To further validate the concept, FO-MD hybrid experiments were conducted with integrated FO-MD setup (see details in section 2.1 and 2.4). It can be seen in **Figure 13b** that MD fluxes were dependent upon the FO fluxes. Streams which produced good FO fluxes resulted in higher MD fluxes like 10.86 LMH and 11.12 LMH with DE and RO reject, respectively. Conductivity of permeate remained below 50 µS/cm for three feed streams except for 3PS for which a jump to 436 µS/cm was observed after 13 hours of operation, suggesting partial pore wetting. This probably happened due to higher concentration of oil and grease (32 mg/L) in 3PS feed stream which reduced the FO flux to an average value of 4.83 LMH. This caused the concentration factor of WO solution (MD FS) to increase up to 1.17 instead of decreasing (below 1.0) like for the other three streams. At higher CF extensive scaling took place which resulted in partial pore wetting and increased the conductivity of permeate. Extensive scaling can be observed in the SEM image in **Figure 14** and EDX images in **Figure S5f** (supporting information). The sustainable operation of the FO-MD hybrid system was successfully presented with the selected

experimental conditions in this section. Moreover the experimental results were able to provide an insight on a continuous operation of an FO-MD hybrid system.

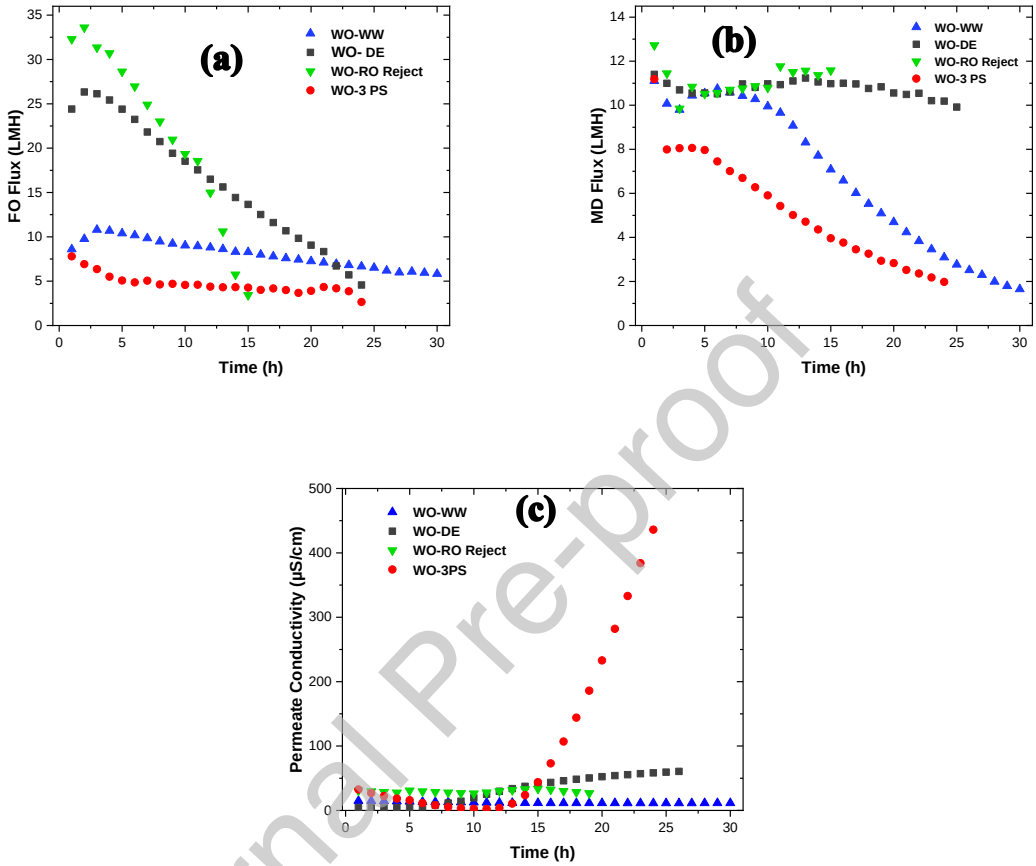

Figure 13: (a) FO flux, (b) MD flux and (c) permeate conductivity during FO-MD hybrid experiments using integrated FO-MD module.

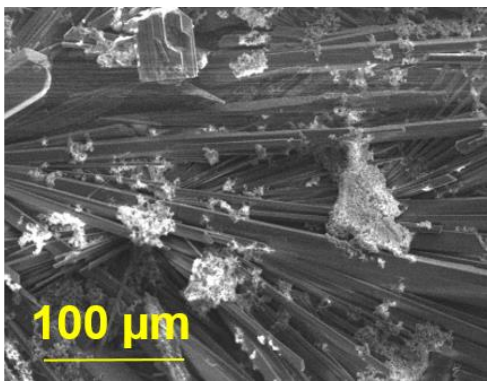

Figure 14: SEM image of active layers of MD membranes during FO-MD hybrid experiments with WO as MD FS using integrated FO-MD module.

3.5. Quality and reuse of product water stream

Results of MD permeate quality presented in **Table 4** shows that it is very high in quality and rejection of different salts and organics was generally above 99%. Comparable rejections for inorganic and organic compounds (98-99%, respectively) is reported in the literature (Ding et al., 2020; Gryta, 2020). A slight reduction in pH of the product water from initial to the end of each experiment was observed which is described in **Table 4**. It can be explained with the fact that DI water was used as MD coolant which is purified to the highest standards with absence of organics, inorganic, dissolved species, particulate matter, volatile contaminants and dissolved gases. This property makes this water an excellent solvent that can dissolve atmospheric carbon dioxide to form carbonic acid which can lower the pH of the permeate solution down to 4 (Alpatova et al., 2020). Average conductivities of MD permeate are also mentioned in **Table 4** and they were mostly below 35 µS/cm, which reflects a very good quality. Initial and final CODs of permeate were always zero confirming no transfer of organics across the membrane.

Table 4: Characteristics of permeate for all MD and hybrid FO-MD experiments

Experiment	Initial pH	Final pH	Average Cond. (µS/cm)	Final COD (mg/L)
WO 50-20	7.84	7.73	14.77	0.0
WO 60-20	7.88	7.83	9.65	0.0
WO 70-20	7.74	7.96	20.23	0.0
NaCl 60-20	7.60	7.54	13.99	0.0

NaCl 70-20	7.71	7.75	12.09	0.0
HA 20	7.9	6.79	22.65	0.0
HA 60	7.7	7.96	1.65	0.0
HA 80	8.2	6.8	3.30	0.0
HA 20 + O&G 30	7.75	7.64	14.05	0.0
HA 20 + O&G 40	8.28	7.5	4.70	0.0
HA 20 + O&G 50	7.96	7.11	1.84	0.0
HA 20 + O&G 40 + EDTA 0.001 M	8.07	6.69	24.85	0.0
HA 20 + O&G 40 + EDTA 0.0005 M	8.60	5.65	10.35	0.0
FO-MD hybrid WO-WW	8.65	8.39	13.0	0.0
FO-MD hybrid WO-DE	7.65	7.28	32.5	0.0
FO-MD hybrid WO-3PS	8.32	7.12	436	0.0
FO-MD hybrid WO-RO reject	8.52	8.14	8.0	0.0

As per Royal commission standards, the storage capacity for untreated wastewater must be of 3 days at industrial sites. So, the concentration of feed streams will reduce the volume of storage reservoirs. Also, the concentrated feed streams can be sent to the evaporation ponds or mineral recovery technologies to extract water and useful minerals. The product water easily meets Royal commission standards for water quality discharge to coastal waters and irrigation water quality standards (Environmental control department, 2004).

4. Conclusions

In this study, a novel FO-MD hybrid for the treatment of produced water was experimentally validated. It enabled simultaneous treatment and reuse of different streams available at the same

industrial oil extraction site. These streams include effluents from desalter, separator and RO treatment equipment, which all contribute to the final WO volume. The WO stream (97 g/L) was used as DS for FO and feed for MD in an integrated hybrid FO-MD system. Using feed water streams with different concentrations (between 4.8 - 6.9 g/L) generated fairly stable FO fluxes ranging between 8.30 LMH and 26.78 LMH. These fluxes were mainly dependent on the composition of feed streams and SRSF was found directly proportional to the concentration of monovalent salts therein. The fouling of the FO membrane resulted from the contribution of different mechanisms to which ICP inside the support layer and ECP on the active layer did contribute significantly. The most dominant mechanism was found to be colloidal calcium silicate scaling on the support layer. On the other hand, MD average flux of 14.41 LMH was achieved while treating the WO stream at a feed and permeate temperatures of 60 $^{\circ}$C and 20 $^{\circ}$C, respectively. Pore blocking due to $CaSO_4$ formation stands among the main reasons for MD flux decline. The co-presence of additional humic acid and already available calcium ions in the feed increased the severity of fouling and reduced the flux further by 6% compared to WO flux without humic acid. Furthermore, scale resulting from humic acids and $CaSO_4$ is tenacious and cannot be completely removed from the membrane surface through simple rinsing with DI water. Interestingly, in our standalone MD experiments, the emulsified oil and grease fouling mechanism was partial pore blocking without wetting, with only 2% flux decline. A complete MD flux recovery was possible by using EDTA to partially mask the divalent calcium ions and reduce the dissociation of humic acids. However, in integrated FO-MD experiments, the MD flux was linked to the FO flux directly. With DE and RO reject as FS streams, WO produced stable MD fluxes of 10.86 LMH and 11.12 LMH, respectively. Product water has zero COD and typical pH (7 ± 1.3) with conductivity <35 µS/cm and can be used for various industrial

purposes. Further investigations in this area like pre-treatment methods, validation with real produced water streams and membrane cleaning methods are recommended.

Acknowledgements

The research reported in this paper was supported by King Abdullah University of Science and Technology (KAUST), Saudi Arabia through a sponsored research project by Saudi Aramco, Grant # RGC/3/3598-01-01. The help, assistance and support of the Water Desalination and Reuse Center (WDRC) staff is greatly appreciated.

References

Ahmed, S.A., Koleshwar, V.S., Yousef, K.K., Albluwi, S.F. and Owaidhi, S.H. 2020 Saudi Aramco Drives Technological Initiatives for Groundwater Conservation In Oil & Gas Production Facilities, p. 14, International Petroleum Technology Conference, Dhahran, Kingdom of Saudi Arabia.

Akther, N., Sodiq, A., Giwa, A., Daer, S., Arafat, H.A. and Hasan, S.W. 2015. Recent advancements in forward osmosis desalination: A review. Chemical Engineering Journal 281, 502.

Al-Furaiji, M., Benes, N., Nijmeijer, A. and McCutcheon, J.R. 2019. Use of a Forward Osmosis-Membrane Distillation Integrated Process in the Treatment of High-Salinity Oily Wastewater. Industrial & Engineering Chemistry Research 58(2), 956-962.

Al-Ghouti, M.A., Al-Kaabi, M.A., Ashfaq, M.Y. and Da'na, D.A. 2019. Produced water characteristics, treatment and reuse: A review. Journal of Water Process Engineering 28, 222-239.

Al Hawli, B., Benamor, A. and Hawari, A.A. 2019. A hybrid electro-coagulation/forward osmosis system for treatment of produced water. Chemical Engineering and Processing - Process Intensification 143.

Alkhudhiri, A., Darwish, N. and Hilal, N. 2013. Produced water treatment: Application of Air Gap Membrane Distillation. Desalination 309, 46-51.

Alpatova, A., Qamar, A., Al-Ghamdi, M., Lee, J. and Ghaffour, N. 2020. Effective membrane backwash with carbon dioxide under severe fouling and operation conditions. Journal of Membrane Science 611, 118290.

Alsaadi, A.S., Francis, L., Maab, H., Amy, G.L. and Ghaffour, N. 2015. Evaluation of air gap membrane distillation process running under sub-atmospheric conditions: Experimental and simulation studies. Journal of Membrane Science 489, 73-80.

APHA 2006. Standard Methods for the Examination of Water and Wastewater. 20th Edition.

Arcanjo, G.S., Costa, F.C.R., Ricci, B.C., Mounteer, A.H., de Melo, E.N.M.L., Cavalcante, B.F., Araújo, A.V., Faria, C.V. and Amaral, M.C.S. 2020. Draw solution solute selection for a hybrid forward osmosis-membrane distillation module: Effects on trace organic compound rejection, water flux and polarization. Chemical Engineering Journal 400, 125857.

Bagheri, M., Roshandel, R. and Shayegan, J. 2018. Optimal selection of an integrated produced water treatment system in the upstream of oil industry. Process Saf Environ 117, 67-81.

Bell, E.A., Poynor, T.E., Newhart, K.B., Regnery, J., Coday, B.D. and Cath, T.Y. 2017. Produced water treatment using forward osmosis membranes: Evaluation of extended-time performance and fouling. Journal of Membrane Science 525, 77-88.

Bhinder, A., Fleck, B.A., Pernitsky, D. and Sadrzadeh, M. 2015. Forward osmosis for treatment of oil sands produced water: systematic study of influential parameters. Desalination and Water Treatment 57(48-49), 22980-22993.

Chang, H., Li, T., Liu, B., Vidic, R.D., Elimelech, M. and Crittenden, J.C. 2019. Potential and implemented membrane-based technologies for the treatment and reuse of flowback and produced water from shale gas and oil plays: A review. Desalination 455, 34-57.

Chekli, L., Kim, Y., Phuntsho, S., Li, S., Ghaffour, N., Leiknes, T. and Shon, H.K. 2017. Evaluation of fertilizer-drawn forward osmosis for sustainable agriculture and water reuse in arid regions. J Environ Manage 187, 137-145.

Chekli, L., Pathak, N., Kim, Y., Phuntsho, S., Li, S., Ghaffour, N., Leiknes, T. and Shon, H.K. 2018. Combining high performance fertiliser with surfactants to reduce the reverse solute flux in the fertiliser drawn forward osmosis process. J Environ Manage 226, 217-225.

Dickhout, J.M., Moreno, Y., Biesheuvel, P.M., Boels, L., Lanuertink, R.G.H. and de Vos, W.M. 2017. Produced water treatment by membranes: A review from a colloidal perspective. J Colloid Interf Sci 487, 523-534.

Ding, C., Zhang, X., Xiong, S., Shen, L., Yi, M., Liu, B. and Wang, Y. 2020. Organophosphonate draw solution for produced water treatment with effectively mitigated membrane fouling via forward osmosis. Journal of Membrane Science 593.

Elmaleh and Ghaffour, N. 1996. Cross-flow ultrafiltration of hydrocarbon and biological solid mixed suspensions. Journal of Membrane Science 118, 111-120.

Environmental control department, K.o.S.A. 2004. Royal commission environmental regulations.

Ghaffour, N. and Qamar, A. 2020. Membrane fouling quantification by specific cake resistance and flux enhancement using helical cleaners. Separation and Purification Technology 239, 116587.

Ghaffour, N., Soukane, S., Lee, J.G., Kim, Y. and Alpatova, A. 2019. Membrane distillation hybrids for water production and energy efficiency enhancement: A critical review. Appl Energ 254, 113698.

Gryta, M. 2020. Separation of saline oily wastewater by membrane distillation. Chemical Papers 74(7), 2277-2286.

Han, L., Xiao, T., Tan, Y.Z., Fane, A.G. and Chew, J.W. 2017. Contaminant rejection in the presence of humic acid by membrane distillation for surface water treatment. Journal of Membrane Science 541, 291-299.

Hou, D., Zhang, L., Wang, Z., Fan, H., Wang, J. and Huang, H. 2015. Humic acid fouling mitigation by ultrasonic irradiation in membrane distillation process. Separation and Purification Technology 154, 328-337.

Jiménez, S., Micó, M.M., Arnaldos, M., Medina, F. and Contreras, S. 2018. State of the art of produced water treatment. Chemosphere 192, 186-208.

Khan, A.A., Khan, I.A., Siyal, M.I., Lee, C.K. and Kim, J.O. 2019. Optimization of membrane modification using SiO2 for robust anti-fouling performance with calcium-humic acid feed in membrane distillation. Environ Res 170, 374-382.

Kim, Y., Li, S., Francis, L., Li, Z.Y., Linares, R.V., Alsaadi, A.S., Abu-Ghdaib, M., Son, H.S., Amy, G. and Ghaffour, N. 2019a. Osmotically and Thermally Isolated Forward Osmosis-Membrane Distillation (FO-MD) Integrated Module. Environ Sci Technol 53(7), 3488-3498.

Kim, Y., Li, S. and Ghaffour, N. 2020. Evaluation of different cleaning strategies for different types of forward osmosis membrane fouling and scaling. Journal of Membrane Science 596, 117731.

Kim, Y., Li, S., Phuntsho, S., Xie, M., Shon, H.K. and Ghaffour, N. 2019b. Understanding the organic micropollutants transport mechanisms in the fertilizer-drawn forward osmosis process. Journal of Environmental Management 248, 109240.

Kim, Y., Woo, Y.C., Phuntsho, S., Nghiem, L.D., Shon, H.K. and Hong, S. 2017. Evaluation of fertilizer-drawn forward osmosis for coal seam gas reverse osmosis brine treatment and sustainable agricultural reuse. Journal of Membrane Science 537, 22-31.

Laqbaqbi, M., Sanmartino, J., Khayet, M., García-Payo, C. and Chaouch, M. 2017. Fouling in Membrane Distillation, Osmotic Distillation and Osmotic Membrane Distillation. Applied Sciences 7(4).

Lee, J. and Ghaffour, N. 2019. Predicting the performance of large-scale forward osmosis module using spatial variation model: Effect of operating parameters including temperature. Desalination 469, 114095.

Lee, J.G., Jang, Y., Fortunato, L., Jeong, S., Lee, S., Leiknes, T. and Ghaffour, N. 2018. An advanced online monitoring approach to study the scaling behavior in direct contact membrane distillation. Journal of Membrane Science 546, 50-60.

Lee, W.J., Ng, Z.C., Hubadillah, S.K., Goh, P.S., Lau, W.J., Othman, M.H.D., Ismail, A.F. and Hilal, N. 2020. Fouling mitigation in forward osmosis and membrane distillation for desalination. Desalination 480.

Li, L., Wang, X., Xie, M., Wang, H., Li, X. and Ren, Y. 2019. EDTA-based adsorption layer for mitigating FO membrane fouling via in situ removing calcium binding with organic foulants. Journal of Membrane Science 578, 95-102.

Li, M., Li, K., Wang, L. and Zhang, X. 2020. Feasibility of concentrating textile wastewater using a hybrid forward osmosis-membrane distillation (FO-MD) process: Performance and economic evaluation. Water Research 172, 115488.

Li, Z. and Demopoulos, G. 2006. Effect of NaCl, MgCl2, FeCl2, FeCl3, and AlCl3 on Solubility of CaSO4 Phases in Aqueous HCl or HCl + CaCl2 Solutions at 298 to 353 K. Journal of Chemical Engineering Data 51, 569-576.

Li, Z.Y., Linares, R.V., Bucs, S., Aubry, C., Ghaffour, N., Vrouwenvelder, J.S. and Amy, G. 2015. Calcium carbonate scaling in seawater desalination by ammonia-carbon dioxide forward osmosis: Mechanism and implications. Journal of Membrane Science 481, 36-43.

Liu, J., Li, Z., Wang, Y., Liu, X., Tu, G. and Li, W. 2021. Analyzing Scaling Behavior of Calcium Sulfate in Membrane Distillation via Optical Coherence Tomography. Water Research, 116809.

Macedonio, F., Ali, A., Poerio, T., El-Sayed, E., Drioli, E. and Abdel-Jawad, M. 2014. Direct contact membrane distillation for treatment of oilfield produced water. Separation and Purification Technology 126, 69-81.

Nawaz, M.S., Parveen, F., Gadelha, G., Khan, S.J., Wang, R. and Hankins, N.P. 2016. Reverse solute transport, microbial toxicity, membrane cleaning and flux of regenerated draw in the FO-MBR using a micellar draw solution. Desalination 391, 105-111.

Politano, A., Argurio, P., Di Profio, G., Sanna, V., Cupolillo, A., Chakraborty, S., Arafat, H.A. and Curcio, E. 2017. Photothermal Membrane Distillation for Seawater Desalination. Adv Mater 29(2).

Ricceri, F., Giagnorio, M., Farinelli, G., Blandini, G., Minella, M., Vione, D. and Tiraferri, A. 2019. Desalination of Produced Water by Membrane Distillation: Effect of the Feed Components and of a Pre-treatment by Fenton Oxidation. Sci Rep 9(1), 14964.

Soliman, M.A., Salu, S., Al-Zahrani, T. and Ansari, N. 2020 Innovative Integrated and Compact Gas Oil Separation Plant for Upstream Surface Facilities, p. 10, Offshore Technology Conference, Houston, Texas, USA.

Son, H.S., Kim, Y., Nawaz, M.S., Al-Hajji, M.A., Abu-Ghdaib, M., Soukane, S. and Ghaffour, N. 2021. Impact of osmotic and thermal isolation barrier on concentration and temperature polarization

and energy efficiency in a novel FO-MD integrated module. Journal of Membrane Science 620, 118811.

Soukane, S., Elcik, H., Alpatova, A., Orfi, J., Ali, E., AlAnsary, H. and Ghaffour, N. 2021. Scaling sets the limits of large scale membrane distillation modules for the treatment of high salinity feeds. Journal of Cleaner Production 287, 125555.

Su, D.L., Wang, J.L., Liu, K.W. and Zhou, D. 2007. Kinetic performance of oil-field produced water treatment by biological aerated filter. Chinese J Chem Eng 15(4), 591-594.

Tanudjaja, H.J., Hejase, C.A., Tarabara, V.V., Fane, A.G. and Chew, J.W. 2019. Membrane-based separation for oily wastewater: A practical perspective. Water Res 156, 347-365.

Tong, T.Z. and Elimelech, M. 2016. The Global Rise of Zero Liquid Discharge for Wastewater Management: Drivers, Technologies, and Future Directions. Environ Sci Technol 50(13), 6846-6855.

Viet, D., Im, S.J. and Jang, A. 2020. Characterization and control of membrane fouling during dewatering of activated sludge using a thin film composite forward osmosis membrane. Journal of Hazardous Materials 396.

Volpin, F., Chekli, L., Phuntsho, S., Ghaffour, N., Vrouwenvelder, J.S. and Shon, H.K. 2019. Optimisation of a forward osmosis and membrane distillation hybrid system for the treatment of source-separated urine. Separation and Purification Technology 212, 368-375.

Wenzlick, M. and Siefert, N. 2020. Techno-economic analysis of converting oil & gas produced water into valuable resources. Desalination 481, 114381.

Xie, M. and Gray, S.R. 2016. Gypsum scaling in forward osmosis: Role of membrane surface chemistry. Journal of Membrane Science 513, 250-259.

Xie, M., Price, W.E., Nghiem, L.D. and Elimelech, M. 2013. Effects of feed and draw solution temperature and transmembrane temperature difference on the rejection of trace organic contaminants by forward osmosis. Journal of Membrane Science 438, 57-64.

Xu, J., Srivatsa Bettahalli, N.M., Chisca, S., Khalid, M.K., Ghaffour, N., Vilagines, R. and Nunes, S.P. 2018. Polyoxadiazole hollow fibers for produced water treatment by direct contact membrane distillation. Desalination 432, 32-39.

Yan, Z., Yang, H., Qu, F., Yu, H., Liang, H., Li, G. and Ma, J. 2017. Reverse osmosis brine treatment using direct contact membrane distillation: Effects of feed temperature and velocity. Desalination 423, 149-156.

Zarga, Y., Ben Boubaker, H., Ghaffour, N. and Elfil, H. 2013. Study of calcium carbonate and sulfate co-precipitation. Chemical Engineering Science 96, 33-41.

Graphical Abstract